Available online at www.sciencedirect.com
SCIENCE DIRECT®
International Journal of Thermal Sciences 42 (2003) 1105–1113
International Journal of Thermal Sciences
www.elsevier.com/locate/ijts

Two-dimensional laminar fluid flow and heat transfer in a channel with a built-in heated square cylinder

Said Turki [a,*], Hassen Abbassi [a], Sassi Ben Nasrallah [b]

[a] *Faculté des sciences de Sfax, département de physique, route de Soukra, BP 802, 3018 Sfax, Tunisia*
[b] *École nationale d'ingénieurs de Monastir, route de Kairouan, 5000 Monastir, Tunisia*

Received 9 September 2002; accepted 11 March 2003

Abstract

A numerical investigation was conducted to analyze the unsteady flow field and heat transfer characteristics in a horizontal channel with a built-in heated square cylinder. Hydrodynamic behavior and heat transfer results are obtained by the solution of the complete Navier–Stokes and energy equations using a control volume finite element method (CVFEM) adapted to the staggered grid. The Computation was made for two channel blockage ratios ($\beta = 1/4$ and $1/8$), different Reynolds and Richardson numbers ranging from 62 to 200 and from 0 to 0.1 respectively at $Pr = 0.71$. The flow is found to be unstable when the Richardson number crosses the critical value of 0.13. The results are presented to show the effects of the blockage ratio, the Reynolds and the Richardson numbers on the flow pattern and the heat transfer from the square cylinder. Heat transfer correlation are obtained through forced and mixed convection.

Keywords: Laminar channel flow; Square cylinder; Forced convection; Mixed convection; Strouhal number; Heat transfer

1. Introduction

Flow over a bluff body is an important research area in many engineering fields. When the flow passes over the bluff body at a certain Reynolds number, wake is produced that is frequently associated with unsteady and periodic vortex shedding. This problem has been studied in detail in the past, most of the research is directed toward the fluid mechanics studies (Davis et al. [1], Sohankar et al. [2], Breuer et al. [3], ...). However, the mechanism of heat transfer under such unsteady flow in a channel flow with the insertion of a cylinder has not been investigated to the same extent.

In pure forced convection, simulation of steady and unsteady two-dimensional flow around a square cylinder was conducted by Kelkar and Patankar [4]. Their computations showed that the temperature fields in the wake for steady and unsteady flow are quite different. The overall heat transfer from the square cylinder in unsteady flow was almost found the same as that in steady flow. Laminar channel flow obstructed by a square cylinder and the related heat transfer were studied numerically and experimentally by Suzuki et al. [5]. They pointed out that a vortex is generated near the channel in phase with the shedding vortices from the cylinder. They observed that the induced vortex near the heat transfer surface entrains the cooler fluid from the downstream side and that this fluid motion contributes to the enhancement of the wall heat transfer. The influence of vortex shedding on the heat transfer characteristics of the rectangular protruding body was conducted numerically by Shuja et al. [6]. Their results show that the vortex attached to the body enhances the heat transfer while detached vortex lowers the heat transfer from the protruding body. They show also, that the effect of vortex shedding on the temperature distribution farther downstream of the flow is negligible because of the flow mixing. Abbassi et al. [7] carried out a numerical investigation to study the forced convection in a horizontal channel with a built-in triangular prism. They showed that for symmetric flow corresponding to a lower Reynolds numbers ($Re < 45$), the presence of the triangular prism has only a local weak effects on the heat transfer from the channel and on the flow pattern, while, in periodic flow

* Corresponding author.
E-mail addresses: said.turki@fss.rnu.tn (S. Turki), hassen.abbassi@fss.rnu.tn (H. Abbassi), sassi.bennasrallah@enim.rnu.tn (S. Ben Nasrallah).

1290-0729/$ – see front matter
doi:10.1016/S1290-0729(03)00091-7

Nomenclature

A	side length of the square cylinder ..... m
f	dominant frequency ..... s^{-1}
Gr	Grashof number, $= \rho^2 g\alpha(T_h - T_c)A^3/\mu^2$
H	channel width ..... m
$\dot{m}_1$	flow rate between the square cylinder and the lower channel wall
$\dot{m}_2$	flow rate between the square cylinder and the upper channel wall
$\overline{Nu}$	space-averaged Nusselt number: on the transverse surfaces, $= \int_0^1 -(\frac{\partial\theta}{\partial x})_w \,\mathrm{d}y$ on the top or bottom surface, $= \int_0^1 -(\frac{\partial\theta}{\partial y})_w \,\mathrm{d}x$
$\langle\overline{Nu}\rangle$	time and space-averaged Nusselt number on each face of the square cylinder, $= \frac{1}{\tau_2-\tau_1}\int_{\tau_1}^{\tau_2} \overline{Nu}\,\mathrm{d}\tau$
$\langle\overline{Nu}_t\rangle$	global time and space-averaged Nusselt number, $= \sum_{\text{all.faces}} \langle\overline{Nu}\rangle/4$
p	pressure nondimensionalized by ρu_0^2
Re	Reynolds number, $= \rho u_0 A/\mu$
Re_{crit}	critical Reynolds number corresponding to the onset of vortex shedding
Ri	Richardson number, $= Gr/Re^2$
St	Strouhal number, $= fA/u_0$
T	dimensional temperature
u_0	maximum of u-component at the channel inlet ..... $m\cdot s^{-1}$
u, v	velocity components nondimensionalized by u_0
V	velocity vector nondimensionalized by u_0
x, y	cartesian coordinates nondimensionalized by A
x_u	distance from body to inlet
x_d	distance from body to outlet

Greek symbols

α	thermal expansion coefficient
β	blockage ratio, $= A/H$
μ	dynamic viscosity of the fluid ..... $kg\cdot m^{-1}\cdot s^{-1}$
θ	dimensionless temperature, $= (T - T_c)/(T_h - T_c)$
ρ	density of the fluid ..... $kg\cdot m^{-3}$
τ	time nondimensionalized by u_0/A
$\Delta\tau$	dimensionless time step
Δx	dimensionless space step in x-direction
Δy	dimensionless space step in y-direction

Subscripts

av	average
c	cold
h	hot
w	wall

($Re \geqslant 45$), heat transfer from the channel is seen to increase strongly in presence of the triangular prism.

In mixed convection, structures of laminar wakes and heat transfer in a horizontal channel with a built-in square cylinder were studied numerically by Biswas et al. [8]. In their study, the channel walls and the surface of the bluff body have higher temperatures than the incoming flow. Their results show that mixed convection can initiate periodicity and asymmetry in the wake at a lower Re than forced convection alone. They also have found that the mixed convection can enhance the heating of the fluid within the channel up to a certain Gr, and further increase in Gr leads to the deterioration in the heat transfer rate. A numerical investigation was conducted by Lange et al. [9] to study the two-dimensional flow around a heated circular cylinder located in a laminar crossflow. They have showed that the temperature dependence of the fluid properties has an influence on the variation of Nusselt number, drag coefficient and the Strouhal number vs Reynolds number. The laminar vortex shedding of airflow behind a circular cylinder with different heating temperatures was experimentally investigated by Wang et al. [10]. Their results show that the frequency data could be successfully collapsed with the effective temperature for a wide range of cylinder temperatures. An universal relationship between Strouhal number and effective Reynolds was also discussed.

The purpose of the present work is a numerical investigation of forced and mixed convection flow in a two dimensional horizontal channel with a built-in heated square cylinder. The effects of the blockage ratio, the Reynolds and Richardson numbers on aerodynamic and heat transfer characteristics are examined. Preliminary 3D simulations conducted by Breuer et al. [3] have shown that the flow obtained at $Re = 300$ is slightly beyond the limit where 2D simulations can be carried out. For this reason, the largest Reynolds number chosen in our study was $Re = 200$ in order to restrict the study to the 2D flow.

2. Governing equations

The flow is assumed to be unsteady, two-dimensional and laminar. All the physical properties of the fluid are assumed to be constant except the density in the buoyancy term. Using the Boussinesq approximation, the governing dimensionless equations can be written in the following conservative form:

$$\mathrm{div}(V) = 0 \tag{1}$$

$$\frac{\partial u}{\partial \tau} + \mathrm{div}(J_u) = -\frac{\partial p}{\partial x}, \quad J_u = uV - \frac{1}{Re}\mathrm{grad}(u) \tag{2}$$

$$\frac{\partial v}{\partial \tau} + \mathrm{div}(J_v) = -\frac{\partial p}{\partial y} + Ri\,\theta, \quad J_v = vV - \frac{1}{Re}\mathrm{grad}(v) \tag{3}$$

$$\frac{\partial\theta}{\partial\tau} + \mathrm{div}(J_\theta) = 0, \quad J_\theta = \theta V - \frac{1}{Re\,Pr}\mathrm{grad}(\theta) \tag{4}$$

In the above equations the space coordinates, velocities, time and pressure are normalized with respectively the width of the square cylinder A, the maximum velocity at the channel inlet u_0, the characteristic time A/u_0 and the characteristic pressure ρu_0^2. The dimensionless variable

$$\theta = \frac{(T - T_c)}{(T_h - T_c)}$$

refers to suitably defined "hot" and "cold" temperatures.

A no-slip condition was applied as the velocity boundary condition along the solid walls. The inlet velocity profile is parabolic while the exit boundary conditions are chosen to minimize the distortion of the unsteady vortices shed from the cylinder and to reduce perturbations that reflect back in to the domain. A detailed investigation carried out by Abbassi et al. [11] shows that the convective boundary condition (CBC) given by:

$$\frac{\partial\Phi}{\partial\tau} + u_{av}\frac{\partial\Phi}{\partial x} = 0 \tag{5}$$

was found to work very well, where the variable Φ is the dependent variable u, v or θ and u_{av} is the mean channel inlet velocity.

The thermal boundary conditions used here are that the upper and the lower channel walls are specified as adiabatic. The square cylinder is assumed to be isothermally heated at T_h, exchanging heat to the cold fluid flowing around it, which is at a uniform temperature T_c at the channel inlet.

3. Numerical method

The combined continuity, momentum and energy equations were resolved using a modified version of control volume finite-element (CVFEM) of Saabas and Baliga [12], adapted to the staggered grid in which pressure is defined at cell centers and velocity components at cell faces. A shape function describing the variation of the dependant variables u, v and θ is needed to evaluate the flux across the control volume faces. We have assumed a linear and an exponential variations respectively for these variables in the diffusive and in the convective terms of the conservation equations. More details and discussions about CVFEM are available in the works of Prakash [13], Masson et al. [14]. The SIMPLER algorithm was applied to resolve the pressure-velocity coupling. Concerning the time resolution, an implicit schema was used for this study and an alternating direction schema (ADI) was considered for performing the time integration. We note that all results presented below are obtained from our numerical code, described and validated in details in Abbassi et al. [7].

4. Results and discussion

Computations have been carried out for flow around a heated square cylinder inside horizontal channel for two blockage ratios. It is changed as $\beta = 1/4$ and $1/8$ under Reynolds number ranging from 62 to 200 and Richardson number up to 0.1 when the Prandtl number is kept constant at 0.71. The square cylinder is symmetrically placed in the channel axis as indicated in Fig. 1. The upstream face of the square cylinder is located at distance $x_u = 10$ from the inlet. The distance from body to outlet is set at $x_d = 15$. Values of x_u and x_d are those recommended by Sohankar et al. [2]. In their study, they show that for the convective boundary convection, the suitable value of x_d seems to be 10 units and for safety reasons, they recommend 15 units, especially at $Re < 100$ for which the recirculation region behind the body is larger and the flow is more viscous.

Computations were performed using 122×57 and 122×77 non uniform meshes for $\beta = 1/4$ and $1/8$ respectively with a variable grid sizes $0.017 \leqslant \Delta x \leqslant 0.6$ and $0.017 \leqslant \Delta y \leqslant 0.2$. In the regions near the solid walls, the grid was made finer by using an exponential stretch described in detail in the work of Turki et al. [15]. The number of nodes distributed over unit length of the square cylinder surface is chosen as Sohanker et al. [2] equal to 20.

In order to study the grid independence, one case was run with 252×137 grid points with $0.008 \leqslant \Delta x \leqslant 0.3$ and $0.008 \leqslant \Delta y \leqslant 0.1$ for $Re = 200$ and $\beta = 1/4$. For this case, 40 nodes are distributed over unit length of the square cylinder surface. The computation results show a difference of only 7% and 8.7% in the values of the Strouhal number St and the global time-averaged Nusselt number $\langle\overline{Nu}_t\rangle$ respectively. St has been calculated using the fast Fourier transform (FFT) of the time trace of the velocity stored downstream at $x = 0.3$ from the square cylinder on the axis channel. It is noted that St and $\langle\overline{Nu}_t\rangle$ seem to be a very stringent basis parameters to be used for the grid independence study. Since the computation time with 252×137 grids is nearly 5 times that with 122×57 grids, the computation with 252×137 is abandoned in favor of 122×57. A sample grid containing 122×57 internal control nodes is shown in Fig. 2 for $\beta = 1/4$.

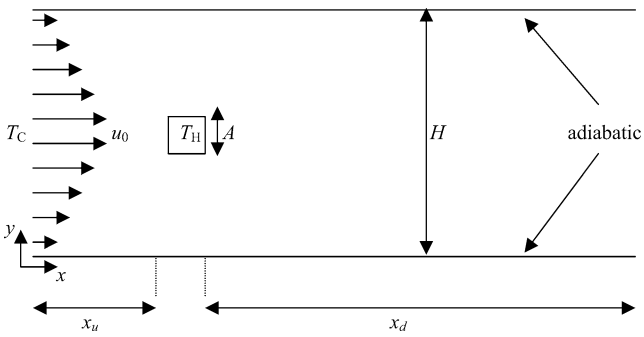

Fig. 1. Configuration definition.

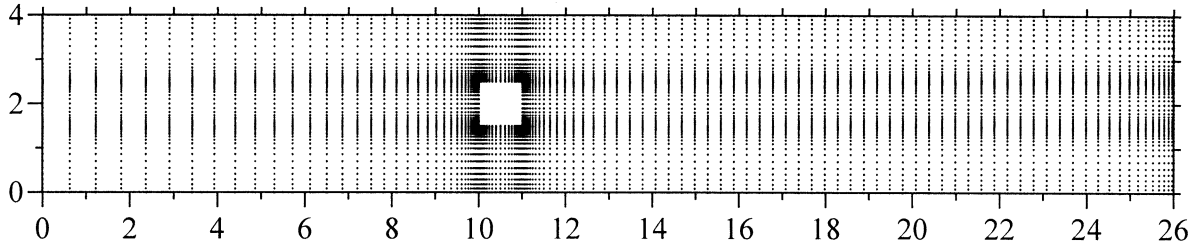

Fig. 2. Non-uniform grid structure for $\beta = 1/4$.

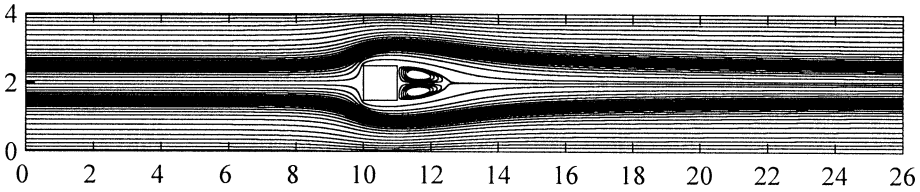

Fig. 3. Streamlines crossing the square cylinder in the channel at $Re = 50$ and $\beta = 1/4$.

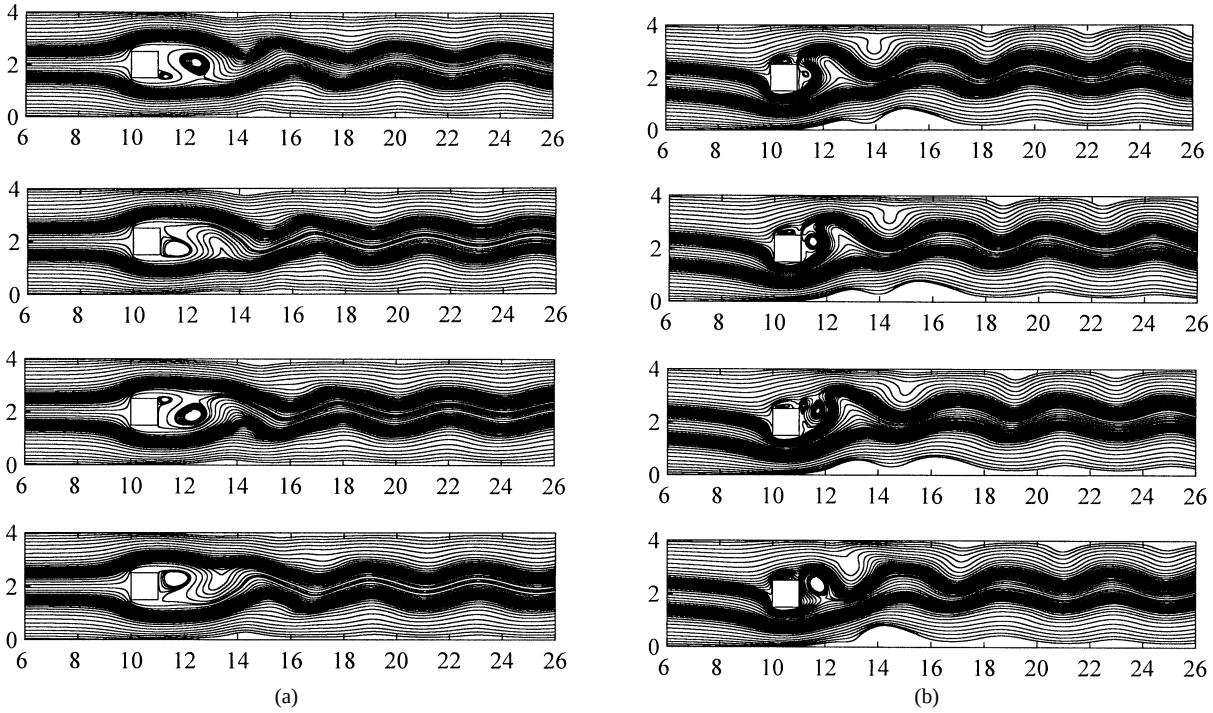

Fig. 4. Streamlines crossing the square cylinder in the channel per cycle of vortex shedding at $Re = 150$ and $\beta = 1/4$ (time interval $= \frac{\Omega}{4}$) ((a) $Ri = 0$, (b) $Ri = 0.044$).

The conditions necessary to prevent numerical instabilities are determined from the combination of Courant–Friedrichs–Lewy (CFL) condition and the restriction on the grid Fourier number. According to the CFL conditions, the distance of the fluid travels in one time increment must be less than one space increment (Δx or Δy) and leads to the constraint on the time step $\Delta\tau$ as:

$$\Delta\tau < \left\{ \frac{\Delta x}{|u|}, \frac{\Delta y}{|v|} \right\} \tag{6}$$

From this condition, the time step employed in the following computation is of the order $\Delta\tau = 0.01$. A time step of $\Delta\tau = 0.005$ does not carry any change on the numerical results.

4.1. *Forced convection* ($Ri = 0$)

In this study, our attention is focused only on the periodic flow characterized by the alternate shedding of vortices from the rear face of the square cylinder into the stream. Basing on the flow visualization as shown in Figs. 3 and 4(a) in which we have presented the streamlines crossing the square cylinder in the channel at $Re = 50$ and $Re = 150$ respectively for $\beta = 1/4$, each characterizes a totally

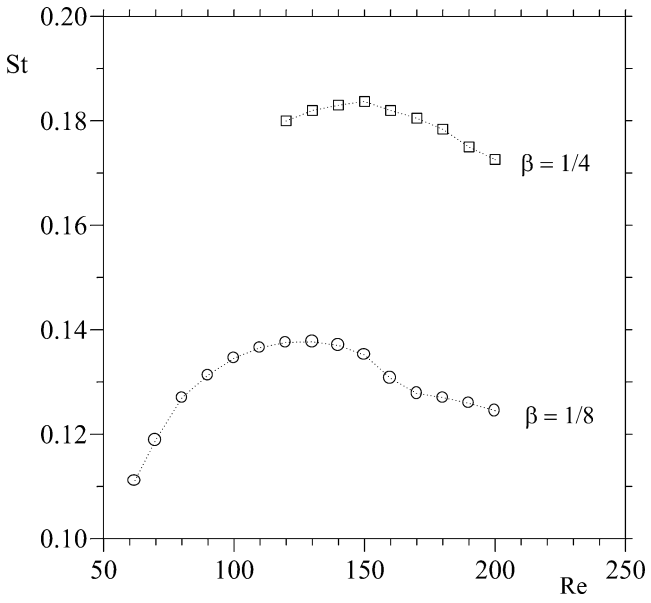

Fig. 5. Effect of blockage ratio on variation in *St* with *Re*.

different flow regime (symmetrical and periodic flows), the onset of vortex shedding was observed at the critical values of Reynolds numbers $Re_{\text{crit}} = 62$ and 120 for $\beta = 1/8$ and $1/4$, respectively. One may conclude that an increase in the blockage ratio leads to an increase in the critical values of *Re* relative to transition from steady to periodic flow. It should be noted that for one cycle of vortex shedding, the starting and ending instants lead to identical flow field, then figure corresponding to the ending instant is to be omitted.

The computed variation of Strouhal number with Reynolds number and blockage ratio is shown in Fig. 5. As it can be noticed, the Strouhal numbers have been found more important for $\beta = 1/4$ as compared to those obtained for $\beta = 1/8$. The difference is about 30 to 40%, then as mentioned by Davis et al. [1] and Sohankar et al. [2] that an increase in the blockage ratio should lead to an increase in the Strouhal number. At the beginning of the periodic flow and for each blockage ratio, the Strouhal number increases when we increase Reynolds number. It reaches a maximum at $Re \approx 130$ and 150 for $\beta = 1/8$ and $1/4$ respectively and then decreases.

The temperature contours in the fluid around the body for $Re = 150$ and $\beta = 1/4$ are displayed in Fig. 6(a) for one cycle of vortex shedding. The high temperature gradient is visible from the contours especially near the front face which have the thinner thermal boundary layers, then the highest heat transfer rates occur near this face. The effect of vortex shedding on the temperature contours is limited to distance $x_T = 7$ (this value corresponds to the contour 0.1) behind the square cylinder for this case, i.e., the temperature contours with high values extend further in the downstream flow developed upon the flow field of the vortex shedding. Further away from the square cylinder, the fluid temperature decreases because of the mixing of the flow in the downstream. In the range of Reynolds number and blockage ratio considered in this study, computation shows that the distance x_T depends on *Re* and β. Increasing *Re* and decreasing β result in decrease in x_T.

Fig. 7 shows the variations of the time-averaged Nusselt number versus Reynolds number on each surface of the square cylinder for $\beta = 1/4$. For each Reynolds number considered in this study, the time-averaged Nusselt number on the bottom face was almost found equal to that of the upper face. Their values decrease slightly with increasing *Re*. The rate of decreasing of $\langle\overline{Nu}\rangle$ from Re_{crit} to $Re = 200$ was found equal to 9%. The front face of the square cylinder has the highest $\langle\overline{Nu}\rangle$ values, followed by the bottom and the rear faces. Contrarily observed on the variation of the $\langle\overline{Nu}\rangle$ versus *Re* on the bottom face, the time-averaged Nusselt number on the front and the rear faces increases with increasing Reynolds number and this enhancement was found more significant for the rear face. Indeed, the rate of increasing $\langle\overline{Nu}\rangle$ from Re_{crit} to $Re = 200$ was found equal to 26% and 77% for the front and the rear faces respectively. For $\beta = 1/8$, similar $\langle\overline{Nu}\rangle(Re)$ curve was also observed on each surface of the square cylinder. The rate of decreasing $\langle\overline{Nu}\rangle$ on the bottom face from Re_{crit} to $Re = 200$ was found equal to 1.6%, the rate of increasing $\langle\overline{Nu}\rangle$ on the front and the rear faces were found equal to 68% and 214% respectively. Throughout those results, it seems that the variation of $\langle\overline{Nu}\rangle$ vs *Re* on the front and the rear faces of the cylinder is more important than that of the bottom and the upper faces. In addition, it is very significant for the rear face.

The global time-averaged Nusselt number $\langle\overline{Nu}_t\rangle$ over the heat transfer surface of the square cylinder is plotted against the Reynolds number in Fig. 8 for $\beta = 1/4$ and $\beta = 1/8$. For a fixed *Re*, the $\langle\overline{Nu}_t\rangle$ slightly increases with a difference less than 5% when β increases from $1/8$ to $1/4$. The slopes of the curves of $\ln(\langle\overline{Nu}_t\rangle)$ versus $\ln(Re)$ was almost found constant in the range of Reynolds number and blockage ratio considered in this study. Starting from the computation results, the global time-averaged Nusselt number can be approximately correlated by the relationships $\langle\overline{Nu}_t\rangle = bRe^a$. The values of the exponent "a" and the coefficient "b" are found as follows:

for $\beta = 1/4$ and $120 \leqslant Re \leqslant 200$:

$$b = 0.939, \qquad a = 0.324$$

for $\beta = 1/8$ and $62 \leqslant Re \leqslant 200$:

$$b = 0.913, \qquad a = 0.323$$

Through those results, it can be shortly concluded that the overall heat transfer from the square cylinder is slightly modified by the blockage ratio. Hence, contrarily to our expectation, it seems that the augmentation of the Strouhal number with the blockage ratio as shown in Fig. 5, has not made a great contribution to the enhancement of heat transfer from the body.

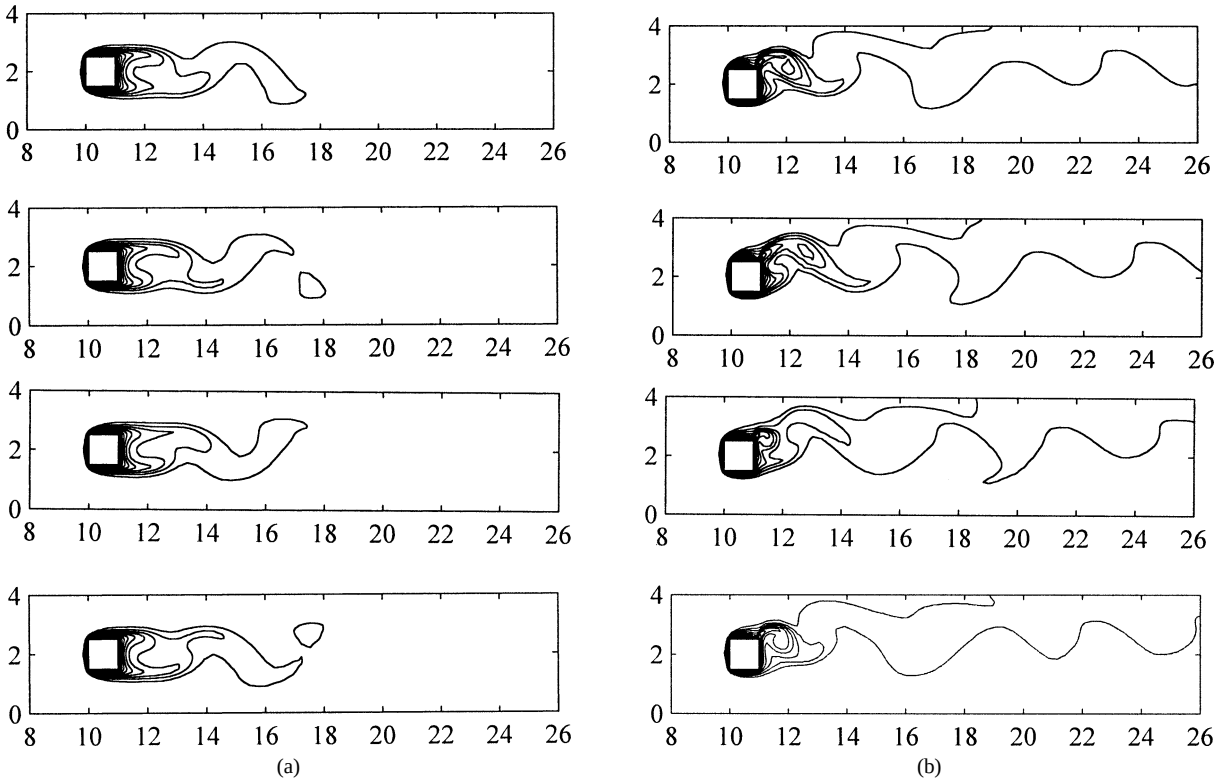

Fig. 6. Temperature contours per cycle of vortex shedding at $Re = 150$ and $\beta = 1/4$ (0.1,[0.1],0.9) ((a) $Ri = 0$, (b) $Ri = 0.044$).

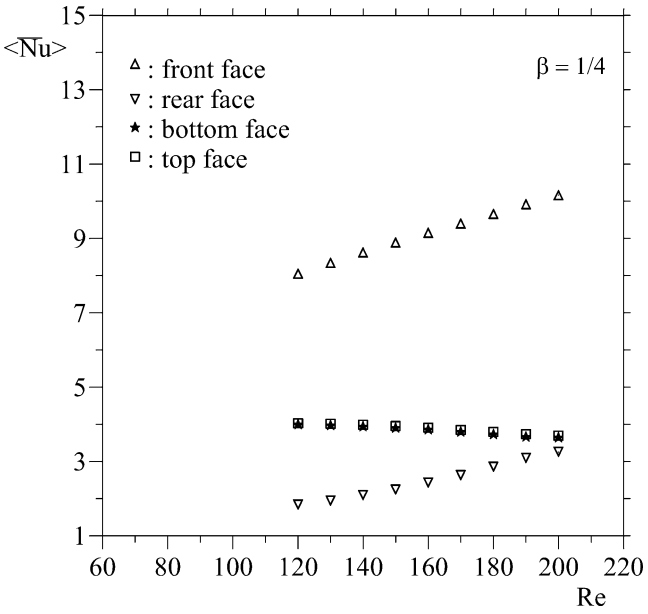

Fig. 7. Variation of $\langle \overline{Nu} \rangle$ vs Re on each faces of the cylinder ($\beta = 1/4$).

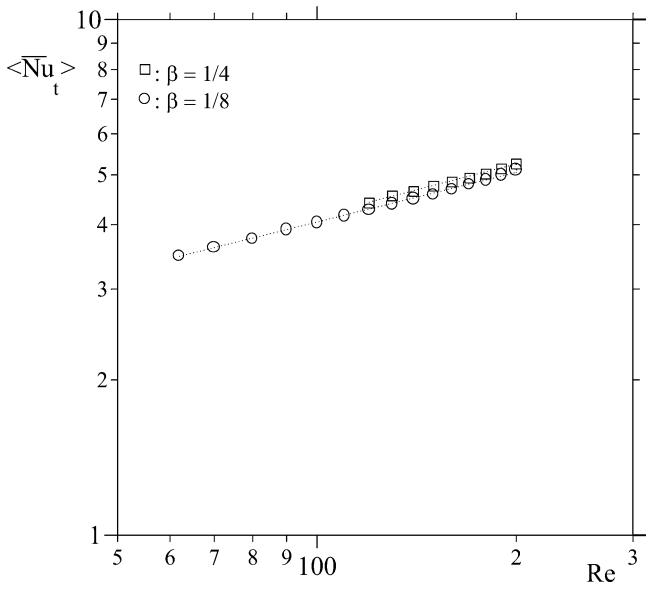

Fig. 8. Variation of $\langle \overline{Nu}_t \rangle$ vs Re for different blockage ratios.

4.2. Mixed convection

In the following of this study, the effect of thermal buoyancy on the flow pattern and the heat transfer characteristics is examined for Ri up to 0.1 and $\beta = 1/4$. The predictions of the present study are given on the basis of the flow field variation and the resulting heat transfer characteristics. It should be noted that the flow was found to be unstable when the Richardson number crosses the value of $Ri = 0.13$.

Fig. 9 shows the effect of buoyancy in the wake region behind the cylinder. For $Re = 100$ and $Ri = 0$ (pure forced convection), the flow is symmetric about the channel axis and vortex shedding has not yet started behind the square cylinder (Fig. 9(a)). For the same Reynolds number and $Ri = 10^{-2}$, the wake loses its original symmetry and the flow

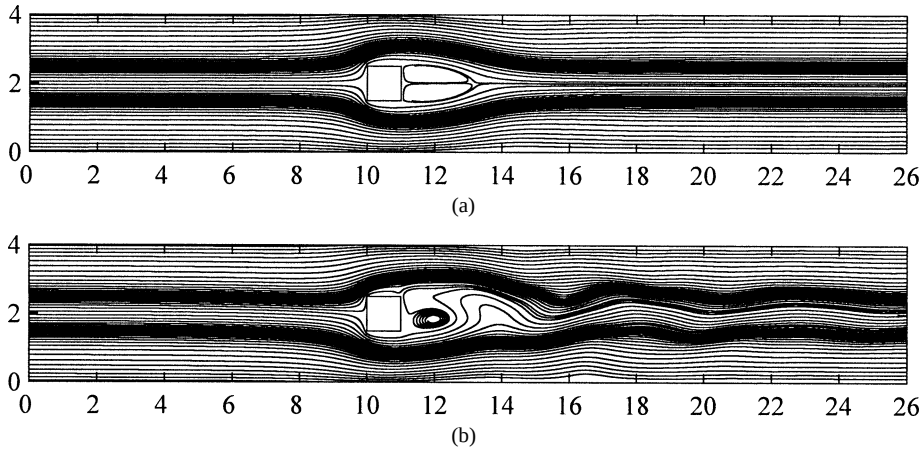

Fig. 9. Streamlines crossing the square cylinder in the channel for $Re = 100$ and $\beta = 1/4$ ((a) $Ri = 0$, (b) $Ri = 0.01$).

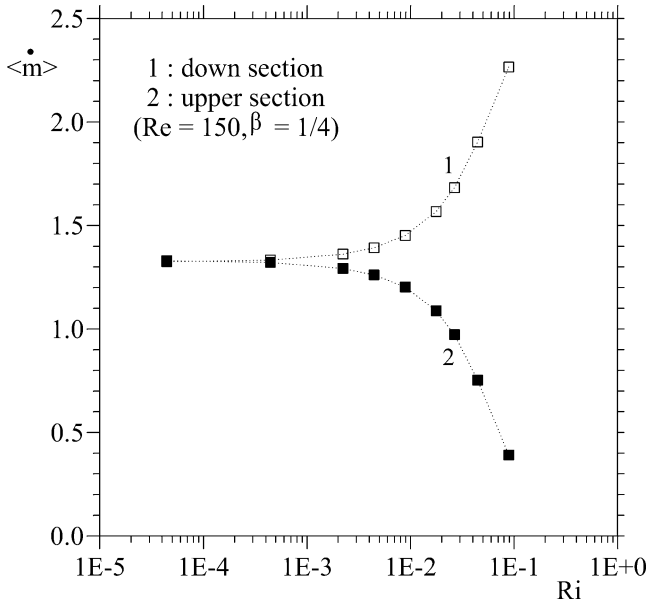

Fig. 10. Variation of the time-averaged flow rate vs *Ri* through the sections between the square cylinder and the channel walls ($Re = 150$ and $\beta = 1/4$).

in the wake becomes periodic (Fig. 9(b)). This periodicity is suppressed in the immediate downstream of the wake. As confirmed by Biswas et al. [8], this result clearly shows that mixed convection can initiate the periodicity in the wake at lower Reynolds numbers than forced convection alone. The critical Reynolds number relative to transition from steady to periodic flow decreases with increasing *Ri*. For example, the critical Reynolds number was found equal to 120, 90 and 70 respectively for $Ri = 0, 10^{-2}$ and 4×10^{-2}.

Fig. 4(b) shows the streamlines crossing the square cylinder in the channel at $Ri = 0.044$ ($Gr = 10^3$ and $Re = 150$). The flow field around the square cylinder shows a different behavior to the flow obtained at $Ri = 0$ (Fig. 4(a): pure forced convection). The first visible effect of the thermal buoyancy is that the vortices which shedding alternately from the rear side of the square cylinder are not symmetrical to the channel axis as observed in pure forced convection. In addition, a recirculation vortex developing a stagnation region near the upper side of the cylinder was observed. Once the Richardson number is increased, the velocity of particle fluids behind the rear face increases and moves toward the upper channel wall. The mass conservation dictates an increased fluid velocity below the square cylinder. As a consequence, when the flow approaches the front face of the cylinder, most of the fluids are flowing below the bottom side of the cylinder. The flow rate which crosses through the section between the square cylinder and the bottom channel wall increases when we increase *Ri*, and it is found more important than that of the one crossing through the section between the square cylinder and the upper channel wall. Fig. 10 confirms this result in which we have presented the time-averaged flow rates of the fluid through the sections between the square cylinder and the channel walls. This figure also shows that for $Ri > 10^{-2}$, the buoyancy effect becomes appreciable and modifies the global structure of the flow around the body. It should be noted as mentioned by Abbassi et al. [11], that in pure forced convection the flow rates through the sections above and below of the cylinder fluctuate in opposition of phase about the half average value of the flow rate at the channel inlet. In addition, the frequency of fluctuation is found to be identical to that of vortex shedding. When increasing The *Ri* number, the two flow rates usually fluctuate in opposition of phase but each other around its average value which is found more important below the square cylinder as shown in Fig. 11.

Fig. 12 compares the Strouhal number against the Reynolds number for different Richardson numbers. For $Ri = 0.05$, a similar behavior of $St(Re)$ curve was found as for pure forced convection ($Ri = 0$) with a maximum at $Re \approx 150$, whereas *St* was found to increase when we increase *Re* and reaches an almost constant level for $Ri = 0.1$. It is noted that $Ri = 0.05$ is beyond the limit where the buoyancy forces become significant. When increasing *Ri* from 0 to 0.05, the Strouhal number slightly increases with a difference less than 10%, whereas an increase of 33% in *St* can be observed between the curves of $Ri = 0.05$ and 0.1 as *Re* reaches 200.

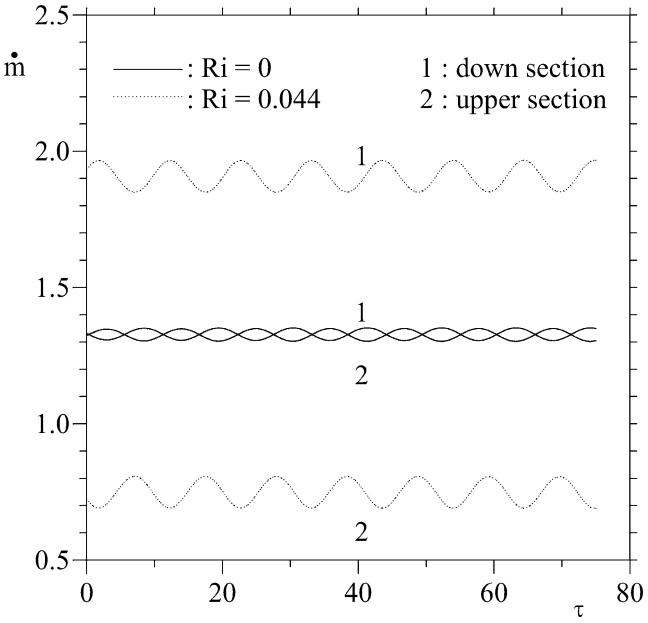

Fig. 11. Evolution of the flow rate with time through the sections between the square cylinder and the channel walls ($Re = 150$ and $\beta = 1/4$).

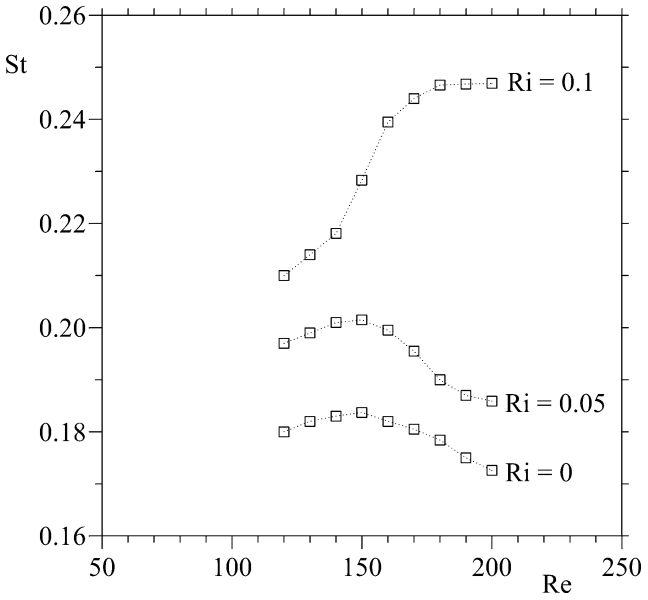

Fig. 12. Variation of *St* vs *Re* for different $Ri(\beta = 1/4)$.

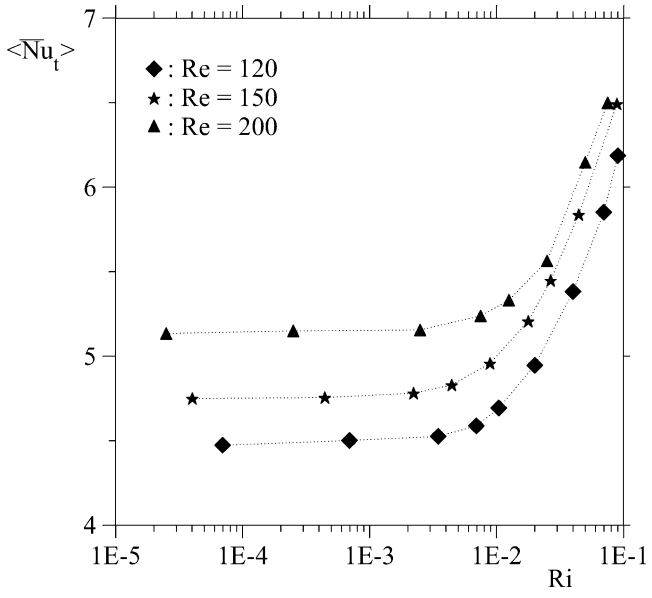

Fig. 13. Variation of $\langle \overline{Nu}_t \rangle$ vs *Ri* for different *Re* ($\beta = 1/4$).

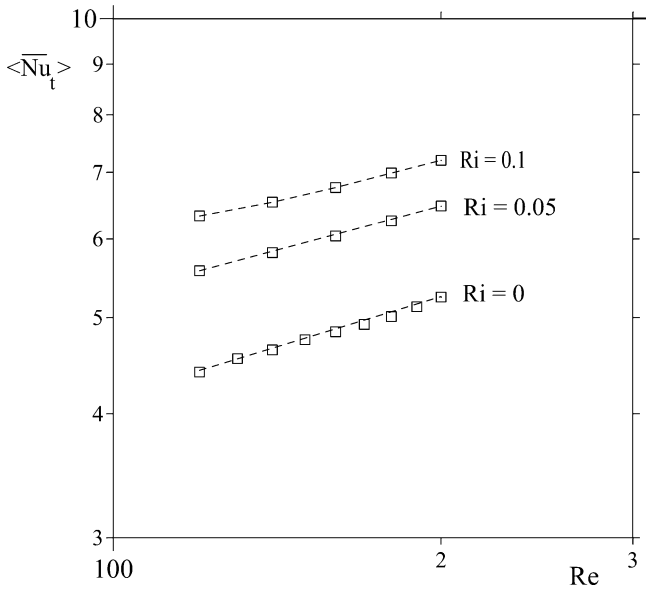

Fig. 14. Variation of $\langle \overline{Nu}_t \rangle$ vs *Re* for different *Ri* ($\beta = 1/4$).

The variations of the global time-averaged Nusselt number as a function of *Ri* at various *Re* is shown in Fig. 13. The ranges of *Ri* in which buoyancy has no effect on the heat transfer are characterized by constant $\langle \overline{Nu}_t \rangle$ values. As it is already observed in Fig. 10, the influence of buoyancy forces becomes more important beyond $Ri = 10^{-2}$. All the curves show a remarkable increase around this value and tend towards an asymptotic value.

Fig. 14 shows the variations of the overall heat transfer from the body with Reynolds number for different Richardson numbers. For a fixed Reynolds number, an increase of 25% and 12% in heat transfer is observed when we pass from $Ri = 0$ to $Ri = 0.05$ and after to $Ri = 0.1$ respectively. All the data for a given *Ri* value are located on a straight-line in a log–log presentation. Therefore, as it is already found in pure forced convection, the global time-averaged Nusselt number can be also correlated by the relationships $\langle \overline{Nu}_t \rangle = c\,Re^a$ in the range of *Ri* up to 0.1. The values of the exponent "*a*" and the coefficient "*c*" are found as follows:

for $Ri = 0$: $c = 0.939$, $a = 0.324$

for $Ri = 0.05$: $c = 1.369$, $a = 0.293$

for $Ri = 0.1$: $c = 1.868$, $a = 0.25$

Finally Fig. 6(b) shows the effect of buoyancy thermal on the temperature contours which show a behavior that

is different from those obtained in forced convection. The isotherm 0.1 is removed far away and tends to be convected toward the upper wall and the exit of the channel, proving hence that the medium flow is more heated in mixed convection than in forced convection.

5. Conclusion

In this paper, we have presented a numerical study to analyze the unsteady flow field and heat transfer characteristics in a horizontal channel with a built-in heated square cylinder. The results can be summarized as follows:

In pure forced convection, the critical value of Reynolds number relative to transition from steady to periodic flow increases when we increase β. The overall heat transfer of the square cylinder was found slightly affected by the blockage ratio and it can be correlated by the following relationships:

for $\beta = 1/4$ and $120 \leqslant Re \leqslant 200$: $\langle \overline{Nu}_t \rangle = 0.939 Re^{0.324}$

for $\beta = 1/8$ and $62 \leqslant Re \leqslant 200$: $\langle \overline{Nu}_t \rangle = 0.913 Re^{0.323}$

In mixed convection, the critical value of Re relative to transition from steady to periodic flow decreases when we increase Ri whereas the Strouhal number St increases with Ri. For $Ri > 10^{-2}$, the flow around the square cylinder was found strongly affected by the thermal buoyancy. The dominant effect observed is the deflection of most of flow toward the bottom of the body. When the thermal buoyancy becomes significant, the heat transfer shows a remarkable increase compared to those obtained in pure forced convection. Finally, for different Ri number considered in this study, the global time-averaged Nusselt number can be also correlated by the relationships: $\langle \overline{Nu}_t \rangle = c\, Re^a$. The values of the exponent "a" and the coefficient "c" are found as follows:

for $Ri = 0$: $c = 0.939$, $a = 0.324$

for $Ri = 0.05$: $c = 1.369$, $a = 0.293$

for $Ri = 0.1$: $c = 1.868$, $a = 0.25$

References

[1] R.W. Davis, E.F. Moore, L.P. Purtell, A Numerical and experimental study of confined flow around rectangular cylinders, Phys. Fluids 27 (1984) 46–59.

[2] A. Sohankar, C. Norberg, L. Davidson, Low-Reynolds number flow around a square cylinder at incidence: Study of blockage, onset of vortex shedding and outlet boundary condition, Internat. J. Numer. Methods Fluids 26 (1998) 39–56.

[3] M. Breuer, J. Bernsdorf, T. Zeiser, F. Durst, Accurate computations of the laminar flow past square cylinder based on two different methods: lattice-Boltzman and finite volume, Internat. J. Heat Fluid Flow 21 (2000) 186–196.

[4] K.M. Kelkar, S.V. Patankar, Numerical prediction of vortex shedding behind a square cylinder, Internat. J. Numer. Methods Fluids 14 (1992) 327–341.

[5] K. Suzuki, H. Suzuki, Unsteady heat transfer in a channel obstructed by an immersed body, Ann. Rev. Heat Transfer 5 (1994) 174–206.

[6] S.Z. Shuja, B.S. Yilbas, M.O. Iqbal, Heat transfer characteristics of flow past a rectangular protruding body, Numer. Heat Transfer Part A 37 (2000) 307–321.

[7] H. Abbassi, S. Turki, S. Ben Nasrallah, Numerical investigation of forced convection in a plane channel with a built-in triangular prism, Internat. J. Therm. Sci. 40 (2001) 649–658.

[8] G. Biswas, H. Laschefski, N.K. Mitra, M. Fiebig, Numerical investigation of mixed convection heat transfer in a horizontal channel with a built-in square cylinder, Numer. Heat Transfer Part A 18 (1990) 173–188.

[9] C.F. Lange, F. Durst, M. Breuer, Momentum and heat transfer from cylinders in laminar crossflow at $10^{-4} \leqslant Re \leqslant 200$, Internat. J. Heat Mass Transfer 41 (22) (1998) 3409–3430.

[10] A.-B. Wang, Z. Travnicek, K.-C. Chia, On the relationship of effective Reynolds number and Strouhal number for the laminar vortex shedding of a heated circular cylinder, Phys. Fluids 12 (6) (2000).

[11] H. Abbassi, S. Turki, S. Ben Nasrallah, Channel flow bluff-body: Outlet boundary condition, vortex shedding and effects of buoyancy, Comput. Mech. 28 (2002) 10–16.

[12] H.J. Saabas, B.R. Baliga, Co-located equal-order control-volume finite element method for multidimensional incompressible fluid flow Part I: Formulation, Numer. Heat Transfer: Part B 26 (1994) 381–407.

[13] C. Prakash, An improved control volume finite-element method for heat and mass transfer and for fluid flow using equal-order velocity-pressure interpolation, Numer. Heat Transfer 9 (1986) 253–276.

[14] C. Masson, H.J. Saabas, B.R. Baliga, Co-located equal-order control-volume finite element method for two-dimensional axisymmetric incompressible fluid flow, Internat. J. Numer. Methods Fluids 18 (1994) 1–26.

[15] S. Turki, G. Lauriat, An examination of two numerical procedures for natural convection in composite enclosures, AIAA/ASME Thermophys. Heat Transfer Conf. ASME-HTD 130 (1990) 107–113.